International Journal of Electrical, Electronic and Communication Sciences
ISSN: 2517-9438
Vol:4, No:8, 2010

# A New Physical Modeling for Multiquantum Well Structure APD Considering Nonuniformity of Electric Field in Active Regin

F. Barzegar, M. H. Sheikhi

***Abstract*—**In the present work we model a Multiquantum Well structure Separate Absorption and Charge Multiplication Avalanche Photodiode (MQW-SACM-APD), while the Absorption region coincide with the MQW. We consider the nonuniformity of electric field using split-step method in active region. This model is based on the carrier rate equations in the different regions of the device. Using the model we obtain the photocurrent, and dark current. As an example, InGaAs/InP SACM-APD and MQW-SACM-APD are simulated. There is a good agreement between the simulation and experimental results.

***Keywords*—**Avalanche Photodiode, Physical Model, Multi-quantum Well, Split Step Method.

## I. Introduction

OVER the past five decades avalanche photodiodes (APD's) have been utilized for a wide range of, commercial military, and research application [1]. Photodiodes with high speed and sensitivity are necessary components in long-haul, high-bit-rate optical communication systems. Avalanche photodiodes are preferred for these systems because their internal gain results in higher [2]-[3]. APD's operate by converting incident absorbed photons into cascades of electron-hole pairs. Specifically, an absorbed photon produces an initial electron-hole pair (parent carriers) within the front-illuminated $p^+$ contact. Due to the action of a reverse-bias field, the hole is immediately swept out of the contact while the electron is accelerated through the depletion region. Under high reverse bias, the electron, on average, attains sufficiently high energy for impact ionization giving rise to a secondary electron-hole pair. The initial and secondary carriers resume their flight through the device during which additional electron-hole pairs are produced. In this way, a cascade of secondary carriers is generated by each incident Photogenerated electron. The multiplication process introduces noise due to fluctuations in the number of secondary carriers created per detected photon [4]. Among the various APD structures presented, the separate absorption, charge and multiplication (SACM) APD is widely deployed. To achieve low bias voltage and low noise, the multiplication and the absorption regions are separated in two different layers, so that the absorption occurs in a layer of narrow band-gap material, while a wider band-gap material is used for the multiplication layer. To increase the gain-bandwidth product, a high electric field is applied to the multiplication layer, and this can be achieved using a charge-sheet layer of high doping density [5]. Until recently, a few analyses and models for SACM-APD's have been reported. But there is a fault in this simulation and modeling. The profile of electric field is not uniform in active regions and is linearly changed. One way to consider these gradual changes is using split-step method in our simulation. In this work a physical modeling is presented for MQW-structure SACM-APD considering nonuniformity of electric field. We split the active region of device into smaller pieces and in different small regions we assume that the profile of electric field is changed step by step. We also calculated Absorption in MQW region. Our modeling is based on the minority carrier equations in different regions of device. Under the considerations of the minority carrier diffusion in side regions ($p^+$, $n^+$) and the carrier drift in the absorption and multiplication regions.

F.Barzegar is with the Electrical Engineering Department, Shiraz University, Shiraz, Iran (Email: fm.barzegar@gmail.com).
M.H.Sheikhi is the head of shiraz university nanotechnology research institute(NRI), Shiraz University, Shiraz, Iran.(Email:msheikhi@shirazu.ac.ir).

## II. Device Structure

The schematic structure of MQW-SACM-APD is shown in Fig.1.This device employ MQW structure in absorption region which composed of alternating layers of very thin nominally undoped $In_{0.53}Ga_{0.47}As$ well-layers and InP barrier-layers. Applying MQW structures increase absorption coefficient. For the sake of convenience, the following deductions are for illumination through ($n^+$) side. The current is equal everywhere in the APD device, so take $p^+$-A and $n^+$-M interfaces for considering $p^+$-A. For the and $n^+$-M interfaces , the current through the interface includes two parts: One is the diffusion current of the minority carriers in the ($n^+$) and ($p^+$) regions and the other is the drift current in *A* and *M* regions. Because of the high electric field, the impact ionization takes place in m region. Also, we assume a little impact ionization in the charge region. According to the actual device, some reasonable suppositions and approximations ations are choosen. 1) The widths of depletion layer in the ($n^+$) and ($p^+$) regions are neglected the electric field is zero in the($n^+$) and ($p^+$) regions. 2) The electric field is uniform in absorption and

multipliation regions. 3) The electric field is nonuniform in charge region and increases as consecutive steps. 4) The multiplication and charge layers are depleted completely. 5) The impact ionization coefficients α and β are assumed to depend only on the local electric field.

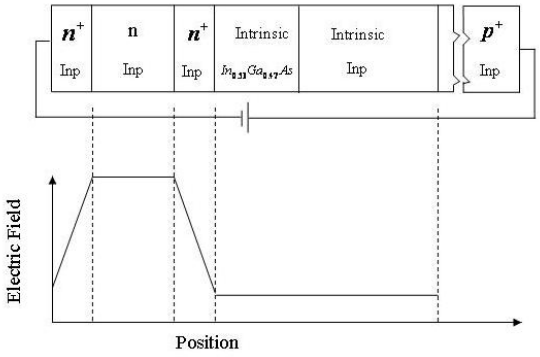


Fig.1.Schematic representation of multiquantum well structure and corresponding electric field profile.

Since the changes of electric field in A and M regions is small and in charge region is very sharp, we can consider that the profile of electric field in A and M regions is uniform and in charge region is linearly changed.

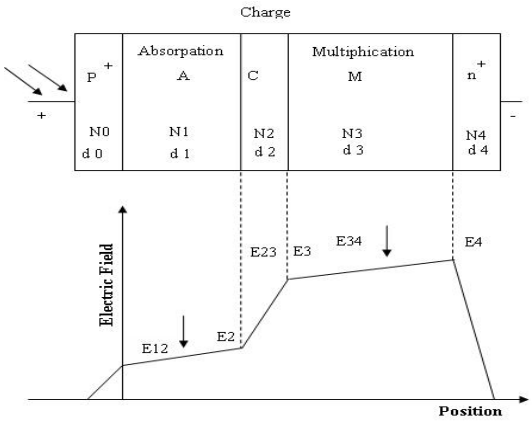


Fig.2 Schematic Structure of SACM-APD

. The field profiles as a function of positions are listed as follows [6]:

We split the charge region into 4 smaller pieces and in different small regions we attribute the average of electric field in each region to any region. This process is shown in Fig.3.

$$E_{12}(x) = \frac{qN_0}{\varepsilon_0 \varepsilon_{S0}} d_0 + \frac{qN_1}{\varepsilon_0 \varepsilon_{S1}}(x) \quad (1)$$

$$E_{23}(x) = \frac{qN_0}{\varepsilon_0 \varepsilon_{S0}} d_0 + \frac{qN_1}{\varepsilon_0 \varepsilon_{S1}} d_1 + \frac{qN_2}{\varepsilon_0 \varepsilon_{S2}}(x - d_1) \quad (2)$$

$$E_{34}(x) = \frac{qN_0}{\varepsilon_0 \varepsilon_{S0}} d_0 + \frac{qN_1}{\varepsilon_0 \varepsilon_{S1}} d_1 + \frac{qN_2}{\varepsilon_0 \varepsilon_{S2}} d_2 + \frac{qN_3}{\varepsilon_0 \varepsilon_{S3}}(x - d_1 - d_2) \quad (3)$$

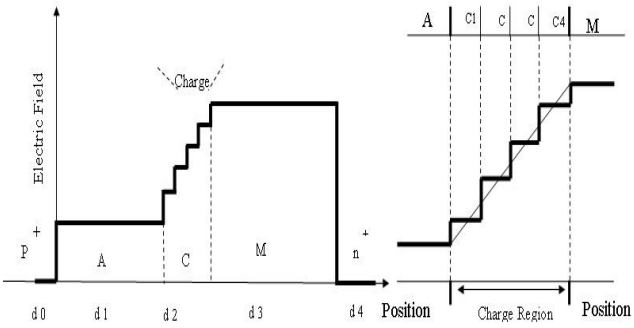


Fig.3. Implementation of split-step method in charge region

## III. Physical Model

### A. Carrier rate equations

For physical modeling, we must deduce the carrier rate equations in the different regions .These are as following [7]: where the $n_{p^+}$ is the total electrons in the ($p^+$) region $p_{c1}$, $p_{c2}$, $p_{c3}$, $p_{c4}$ and $n_{c1}$, $n_{c2}$, $n_{c3}$, $n_{c4}$ are the total holes and electrons in the C region respectively, $p_a$, $p_m$, $n_a$, $n_m$ are total holes and

$p^+$ region:
$$\frac{dn_P}{dt} = -\frac{n_p}{\tau_n} - \frac{I_n}{q} \quad (4)$$

A region:
$$\frac{dn_a}{dt} = N_{Ga} - \frac{n_a}{\tau_{nra}} - \frac{n_a}{\tau_{nta}} + \frac{I_n}{q} \quad (5)$$

$$\frac{dp_a}{dt} = P_{Ga} - \frac{p_a}{\tau_{pra}} - \frac{p_a}{\tau_{pta}} + \frac{I_{cp1}}{q} \quad (6)$$

pc1 region:
$$\frac{dn_{C1}}{dt} = \alpha_{C1}\upsilon_{nC1}.n_{C1} + \beta_{C1}\upsilon_{pC1}.p_{C1} - \frac{n_{C1}}{\tau_{nrC}} - \frac{n_{C1}}{\tau_{ntC1}} + \frac{I_{an}}{q} \quad (7)$$

$$\frac{dp_{C1}}{dt} = \alpha_{C1}\upsilon_{nC1}.n_{C1} + \beta_{C1}\upsilon_{pC1}.p_{C1} - \frac{p_{C1}}{\tau_{prC}} - \frac{p_{C1}}{\tau_{ptC1}} + \frac{I_{cp2}}{q} \quad (8)$$

Pc2 region:
$$\frac{dn_{C2}}{dt} = \alpha_{C2}\upsilon_{nC2}.n_{C2} + \beta_{C2}\upsilon_{pC2}.p_{C2} - \frac{n_{C2}}{\tau_{nrC}} - \frac{n_{C2}}{\tau_{ntC2}} + \frac{I_{cn1}}{q} \quad (9)$$

$$\frac{dp_{C2}}{dt} = \alpha_{C2}\upsilon_{nC2}.n_{C2} + \beta_{C2}\upsilon_{pC2}.p_{C2} - \frac{p_{C2}}{\tau_{prC}} - \frac{p_{C2}}{\tau_{ptC2}} + \frac{I_{cp3}}{q} \quad (10)$$

Pc3 region:
$$\frac{dn_{C3}}{dt} = \alpha_{C3}\upsilon_{nC3}.n_{C3} + \beta_{C3}\upsilon_{pC3}.p_{C3} - \frac{n_{C3}}{\tau_{nrC}} - \frac{n_{C3}}{\tau_{ntC3}} + \frac{I_{cn2}}{q} \quad (11)$$

$$\frac{dp_{C3}}{dt} = \alpha_{C3}\upsilon_{nC3}.n_{C3} + \beta_{C3}\upsilon_{pC3}.p_{C3} - \frac{p_{C3}}{\tau_{prC}} - \frac{p_{C3}}{\tau_{ptC3}} + \frac{I_{cp4}}{q} \quad (12)$$

Pc4 region:

$$\frac{dn_{C4}}{dt} = \alpha_{C4}\upsilon_{nC4}.n_{C4} + \beta_{C4}\upsilon_{pC4}.p_{C4} - \frac{n_{C4}}{\tau_{nrC}} - \frac{n_{C4}}{\tau_{ntC4}} + \frac{I_{cn3}}{q} \quad (13)$$

$$\frac{dp_{C4}}{dt} = \alpha_{C4}\upsilon_{nC4}.n_{C4} + \beta_{C4}\upsilon_{pC4}.p_{C4} - \frac{p_{C4}}{\tau_{prC}} - \frac{p_{C4}}{\tau_{ptC4}} + \frac{I_{mp}}{q} \quad (14)$$

M region:

$$\frac{dn_m}{dt} = \alpha_m\upsilon_{nm}.n_m + \beta_m\upsilon_{pm}.p_m - \frac{n_m}{\tau_{nrm}} - \frac{n_m}{\tau_{ntm}} + \frac{I_{cn4}}{q} \quad (15)$$

$$\frac{dp_m}{dt} = \alpha_m\upsilon_{nm}.n_m + \beta_m\upsilon_{pm}.p_m - \frac{p_m}{\tau_{prm}} - \frac{p_m}{\tau_{ptm}} + \frac{I_p}{q} \quad (16)$$

$n^+$region:

$$\frac{dp_n}{dt} = -\frac{p_n}{\tau_p} - \frac{I_p}{q} \quad (17)$$

electrons through the *A,M* regions and $P_{n^+}$ is the total holes in the ($n^+$) region. *q* is the electron charge, $\tau_n$ and $\tau_p$ are the hole and electron life-time in the ($p^+$) and ($n^+$) regions, $\tau_{prm}$, $\tau_{prc}$, $\tau_{pra}$, $\tau_{nrm}$, $\tau_{nrc}$, $\tau_{nra}$ are the recombination life-time of holes and electron, $\tau_{pta}$, $\tau_{ptc1}$, $\tau_{ptc2}$, $\tau_{ptc3}$, $\tau_{ptc4}$, $\tau_{ptm}$, $\tau_{nta}$, $\tau_{ntc1}$, $\tau_{ntc2}$, $\tau_{ntc3}$, $\tau_{ntc4}$, $\tau_{ntm}$ are the holes and electrons transit times through the *A, P* and *M* regions. In our equations, $I_P$ and $I_n$ are the hole and electron diffusion current in ($n^+$) and ($p^+$) regions, $\nu_n$ and $\nu_p$ are the electron and hole drift velocities and α and β are the electron and hole impact ionization rates and the related equations are in [8]. The currents $I_{cp1}$, $I_{cp2}$, $I_{cp3}$, $I_{cp4}$, $I_{pm}$ result from transition of holes from one layer to adjacent layer $I_{cn1}$, $I_{cn2}$, $I_{cn3}$, $I_{cn4}$, $I_{an}$ and result from transition of electrons from one layer to adjacent layer. These current can be written as follow [7]:

$$I_{mp} = \frac{qp_m}{\tau_{ptm}}, I_{an} = \frac{qn_a}{\tau_{nta}}, I_{cpj} = \frac{qp_{Cj}}{\tau_{ptCj}}, I_{cnj} = \frac{qn_{Cj}}{\tau_{ntCj}} \quad j = 1,2,3,4 \quad (18)$$

$P_{Ga}$ and $N_{Ga}$ are photo-generation rates in absorption region and are defined below [7]:

$$P_{Ga} = N_{Ga} = \frac{P_{in}(1-R_f).\exp[-(a_p.W_p)]}{h\upsilon}.[1-\exp(-a_{ab}.W_a)] \quad (19)$$

Where $P_{in}$ is the optical power, $R_f$ is the reflectivity, and hυ is the photon energy. $a_p$, $a_{ab}$ are the absorption coefficients and $w_p$, $w_a$, $w_{c1}$, $w_{c2}$, $w_{c3}$, $w_{c4}$, $w_m$, $w_n$, are the width of $p^+$, a, $p_1$, $p_2$, $p_3$, $p_4$, m, $n^+$ regions, respectively.

$$\tau_{ptcj} = \frac{W_C/4}{\upsilon_{pcj}}, \tau_{ntcj} = \frac{W_C/4}{\upsilon_{ncj}}, j = 1,2,3,4$$
$$\tau_{pta} = \frac{W_a}{\upsilon_{pa}}, \tau_{nta} = \frac{W_a}{\upsilon_{na}}, \tau_{ptm} = \frac{W_m}{\upsilon_{pm}}, \tau_{ntm} = \frac{W_m}{\upsilon_{nm}} \quad (20)$$

The drift velocity must take the averages in the quantum well region. These can be written as follow [8]:

$$v = \frac{v_w v_b (W_w + W_b)}{v_b W_w + v_w W_b} \quad (21)$$

Where $\zeta_w$, $\zeta_b$, $\nu_w$, $\nu_b$, $W_w$ and $W_b$ are the drift velocities, and widths for well and barrier, respectively. The theoretical current distribution across the entire MQW structure is predicted to be the linear summation of current at each well/barrier interface [9]. We apply the carrier rate equation theory across one well/barrier cell ,(5) and (6). These equations should be written for each well/barrier along whole MQW absorption region. Calculation of absorption coefficient in quantum well region is discussed as follow.

### *B. Absorption coefficient in MQW-Region*

The schematic energy levels band-diagram of a quantum well, as shown in Fig.4. If an electric field is applied perpendicularly to the layers the bands tilt due to the potential of the external field resulting in the shifting of the energy levels as shown in Fig.4(b).

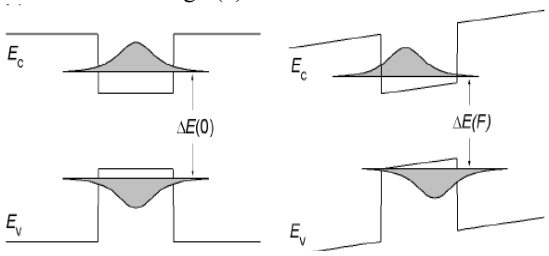


Fig.4. Illustration of the quantum confined Stark effect, quantum well band edges, quantum levels, and wave functions (a) without and (b) with applied electric field .

This results in smaller absorption energy and the absorption edge shifts to longer wavelengths, similar to the Franze-Keldysh effect known from bulk materials. Contrary to the Franz-Keldysh effect, however, the absorption edge retains its steep rise and exciton character. This phenomenon in QW's is referred to as the quantum confined Stark effect (QCSE). It is this steep rise of the absorption edge coupled with a very high excitonic absorption peak which makes this effect so attractive for optoelectronic device. There is an increasing number of device applications in which the QCSE is employed. Light is absorbed by the quantum well when a photon of sufficient energy excites an electron from the valance band into the conduction band, making an electron-hole pair. The lowest energy absorption occurs when the photon creates an electron-hole pair bound together in a state called an "exciton" [10].At

first estimation of the absorption will be obtained, if the bound states of the structure are known. The bound state of a one-dimensional finite potential well are given by the solution of the time-independent Schrodinger equation [11].

$$H\psi = \left( -\frac{\hbar^2}{2m}\frac{\partial^2}{\partial x^2} + v(x) \right)\psi = E\psi \tag{22}$$

Which may be rewritten in the form:

$$\frac{d^2\psi}{dx^2} + \frac{2m}{\hbar^2}\left[E - V(x)\right]\psi(x) = 0 \tag{23}$$

Where V(x) represents the potential energy variation, m is the effective mass of charged particle, and h being Plank's constant. E and ψ respectively represent the energy eigenvalue and eigenfunction of the bound state. The solution of the (22) for a simple square-well and a few other specific forms of V(x) is well known. We now consider a potential energy variation V(x) as shown in Fig.5. Such a structure would have a finite number of bound state corresponding to $V_{min} < E < V$ although all values of $E > V'$ are allowed, we will have a finite number of quasi-bound states corresponding to $V_{min} < E < V$. In order to obtain the eigenvalues corresponding to the bound state and quasi-bound states, we introduce, a region of potential energy which is less than or equal to $V_{min}$ as shown in Fig.5.

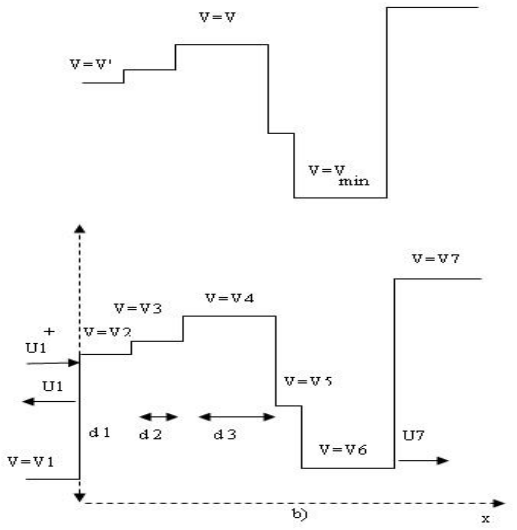


Fig.5. (a) A general potential energy variation having a finite number of bound states (b) our model for the potential energy.

We also choose the region at the point, where we introduced the potential. Referring to Fig.5 the solution of the Schrodinger equation in each region may be written in the form [11]:

$u_i^+$ and $u_i^-$ represent the amplitudes of wave propagating along the +x and –x direction, respectively. Continuity of u and du/dx at each interface gives us:

$$\begin{aligned} u_i &= u_i^+ e^{-i\Delta_i} e^{ik_i x} + u_i^- e^{i\Delta_i} e^{-ik_i x} \\ \Delta_i &= k_1(d_2 + d_3 + \ldots + d_{i-1}); \quad \Delta_1 = \Delta_2 = 0 \\ k_i &= \left[ \frac{2m}{\hbar^2}(E - V_i) \right]^{1/2} \qquad i=3,4,\ldots \end{aligned} \tag{24}$$

$$\begin{bmatrix} u_1^+ \\ u_1^- \end{bmatrix} = S_1 \begin{bmatrix} u_2^+ \\ u_2^- \end{bmatrix} = S_1 S_2 \begin{bmatrix} u_3^+ \\ u_3^- \end{bmatrix} = \ldots\ldots = S_1 S_2 \ldots\ldots S_{N-1} \begin{bmatrix} u_N^+ \\ u_N^- \end{bmatrix} \tag{25}$$

Where

$$\begin{aligned} S_i &= \frac{1}{t_i}\begin{pmatrix} e^{-i\delta_i} & r_i e^{-i\delta_i} \\ r_i e^{i\delta_i} & e^{i\delta_i} \end{pmatrix}, \delta_i = k_i d_i \\ t_i &= \frac{k_i - k_{i+1}}{k_i + k_{i+1}} \end{aligned} \tag{26}$$

i=1, 2, 3, …,N-1,N being the total number of regions. In the last region -Nu would represent an exponentially amplifying solution and should vanish. Setting, -Nu=0 we can calculate the amplitude of the wave function in any region in term of $u_1^+$. By analogy, for the potential energy variation shown in Fig. 5. If we calculate $\frac{u_6^+}{u_1^+}$ as function of E, we would obtain Lorentzians corresponding to each bound state and quasi-bound state of the form [11]:

$$\left| \frac{u_{6^+}}{u_{1^+}} \right|^2 = \frac{\sigma}{(E - E_b)^2 + \theta^2} \tag{27}$$

where $E = E_b'$ represent the position of the peak and 2θ, the full width at half maximum (FWHM). As the distance $d_2$ is increased, $E_b'$ would tend to the value $E_b$ which represent the energy of bound state (or quasi-bound state), the quantity 2θ would tend to zero for bound states and to the nonzero value for quasi- bound state. Thus in order to obtain the energies and lifetimes of the various states of an arbitrarily graded potential well, we adopt the following procedure: 1) We first introduce a region of potential energy equal to or less than the minimum value inside the potential well, beyond the well. 2) Calculating $\left| \frac{u_6^+}{u_1^+} \right|^2$ as a function of E. 3) Fiting a Lorentzian of the form given by (27) and obtain $E_b'$ and θ .4) We let the fictitious region move to ∞ and obtain the limiting values of $E_b'$ and θ, which give the eigenvalue and life time of the bound/quasi-bound state. In practice, the fictitious region is moved sufficiently far from $E_b'$ and θ to converge to required accuracy.We must mention here that an arbitrarily graded potential energy variation can be represented by a large number of steps and solved in a similar manner. However if

there is more than one well in the structure, we have to calculate the ratio $\left|\frac{u_6^+}{u_1^+}\right|^2$ .The optical absorption coefficient can be written as the product of the absorption-exciton peak $\alpha_{hh}$ and a line shape function. The long wave length side of the absorption edge fits a Lorantzian line shape extremely well according to measured data. The following expersion was used for the absorption coefficient [12]:

$$\alpha(E,h\nu,L_z)=\alpha_{hh}\left\{1+\left[\frac{(E_0-h\nu)}{\Gamma_{hh}}\right]^2\right\}^{-1}; \qquad h\nu < E_0 \tag{28}$$

With E0 the energy of hh exciton and $\Gamma_{hh}$ it's FWHM. $E_0$ is, the energy needed to create the exciton and is given by [12]:

$$E_0 = E_g + E_{e1} + E_{h1} - E_B \tag{29}$$

Where $E_g$ is the bulk band gap of the well material, $E_{e1}$ and $E_{h1}$ are the zero-point energies of the electron and hole, respectively, and $E_B$ is the binding energy of the exciton. $\alpha_{hh}$ can be calculated from [12]:

$$\alpha_{hh}(L_z,E)=\frac{C}{L_z}\left|\int_{-\infty}^{\infty}\Psi_e(z)\Psi_h^*(z)dz\right|^2+\alpha_{bulk} \tag{30}$$

The $L_z$ the width of the wells, $\alpha_{bulk}$ is the absorption coefficient of bulk material, $\psi_e$ and $\psi_h$ are the electron and hole wave functions. C is the normalization constant. For calculation of Γ a polynomial fitting curve was used as [12].

$$\Gamma_{hh}(L_Z,E)= 7.34-0.511L_Z+0.018{L_Z}^2-0.054+0.0161E^2 \tag{31}$$

It may seem from (30) the absorption coefficient can be increased by decreasing $L_z$. However, as $L_z$ is decreased , the electron and hole wave functions spread outside the well and the overlap decreases. The reduced overlap results in a corresponding reduction in absorption as shown in Fig.6. Therefore, for every material system there is an optimum well size. For example, for GaAs this $L_z$ ~50A° and for $In_{0.53}Ga_{0.47}As$ $L_z$ ~80A° [13].

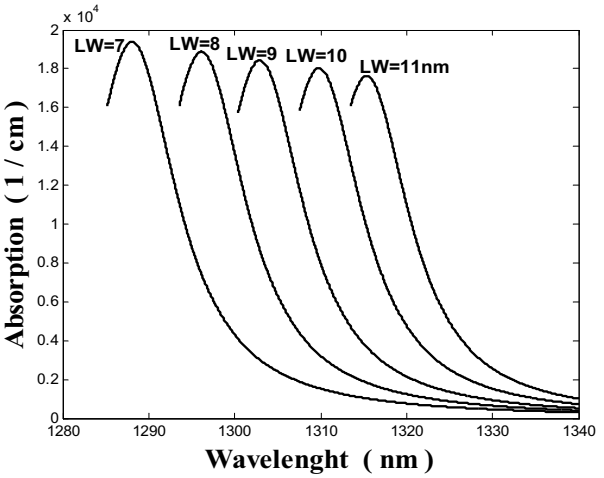


Fig.6. Calculated absorption spectrum in the MQW region at four different wide wells.

Four broadening mechanisms, phonon interaction, tunneling through barrier, well width fluctuation, variation of the electric field over the well are included in.With the application of an electric field several things happen. The electron and hole wave function are separated and pushed toward the opposite sides of the well, as shown in fig. 4(b). The reduced overlap results in a corresponding reduction in absorption and in luminescence as shown in Fig.7.

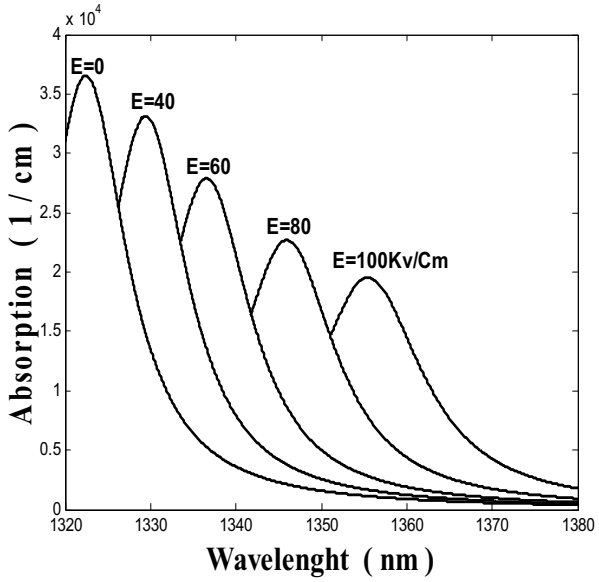


Fig.7. Calculated absorption spectrum in the MQW region by Lorantzian line shape function.

### *C. Photocurrent Calculation*

The current that transit through the device is:

$$I_t = AJ_t \tag{32}$$

$$J_t = \frac{1}{W}\int_0^W [J_e(x)+J_h(x)]dx = \frac{q}{W}\{\int_0^{W_a}\left(\frac{v_{na}.n_a}{AW_a}+\frac{v_{pa}.p_a}{AW_a}\right)dx+$$
$$\int_{w_a}^{W_a+\frac{W_c}{4}}\left(\frac{v_{nc1}.n_{c1}}{A(W_c/4)}+\frac{v_{pc1}.p_{c1}}{A(W_c/4)}\right)dx+\int_{W_a+\frac{W_c}{4}}^{W_a+\frac{W_c}{2}}\left(\frac{v_{nc2}.n_{c2}}{A(W_c/4)}+\frac{v_{pc2}.p_{c2}}{A(W_c/4)}\right)dx$$
$$+\int_{W_a+\frac{W_c}{2}}^{W_a+\frac{3W_c}{4}}\left(\frac{v_{nc3}.n_{c3}}{A(W_c/4)}+\frac{v_{pc3}.p_{c3}}{A(W_c/4)}\right)dx+\int_{W_a+\frac{3W_c}{4}}^{W_a+W_c}\left(\frac{v_{nc4}.n_{c4}}{A(W_c/4)}+\frac{v_{pm}.p_{c4}}{A(W_c/4)}\right)dx$$
$$+\int_{W_a+W_c}^{W_a+W_c+W_m}\left(\frac{v_{nm}.n_m}{AW_m}+\frac{v_{pm}.p_m}{AW_m}\right)dx\}$$

Finally, for this current we have [7]:

$$I_t = I_{ta}+I_{tc}+I_{tm} \tag{33}$$

In this relation we have:

$$I_{ta} = I_{tpa}+I_{tna} = q(\frac{p_a}{\tau_{pta}}+\frac{n_a}{\tau_{nta}}) \tag{34}$$

$$I_{tC} = I_{tpC}+I_{tnC} \tag{35}$$

$$I_{tpC} = I_{tpC1}+I_{tpC2}+I_{tpC3}+I_{tpC4}$$
$$= q(\frac{p_{C1}}{\tau_{ptC1}}+\frac{p_{C2}}{\tau_{ptC2}}+\frac{p_{C3}}{\tau_{ptC3}}+\frac{p_{C4}}{\tau_{ptC4}} \tag{36}$$

$$I_{tnC} = I_{tnC1}+I_{tnC2}+I_{tnC3}+I_{tnC4}$$
$$= q(\frac{n_{C1}}{\tau_{ntC1}}+\frac{n_{C2}}{\tau_{ntC2}}+\frac{n_{C3}}{\tau_{ntC3}}+\frac{n_{C4}}{\tau_{ntC4}}) \tag{37}$$

$$I_{tm} = I_{tpm}+I_{tnm} = q(\frac{p_m}{\tau_{ptm}}+\frac{n_m}{\tau_{ntm}}) \tag{38}$$

The photocurrent of this device can be written as follow:

$$I_{ph} = I_n+I_{tm}+I_{tc}+I_{ta}+I_{dark} \tag{39}$$

$I_n$ is the electron diffusion current in ($p^+$) region and the related equations are in [8].

*1) Dark Current Calculation in Bulk Region*

$I_{dark}$ is the reverse bias dark current and in the charge and multiplication regions is the sum of diffusion $I_{diff}$ tunneling $I_{tun}$ and generation-recombination $I_{gr}$ components. $I_{dark}$ can be written as follows [14]:

$$I_{dark} = I_{diff}+I_{gr}+I_{tun} \tag{40}$$

In these relation we have:

*a) Diffusion Current*

The diffusion current due to thermally generated minority carriers diffusing into the depletion region is given by [14]:

$$I_{diff} = I_S[\exp(\frac{qV}{kT})-1] \tag{41}$$

where $q$ is the electronic charge, $k$ is Boltzmann's constant, T is the junction temperature, and the applied voltage $V$ is negative under reverse bias. The saturation current $I_s$ is [14]:

$$I_S = qn_i^2\left(\sqrt{\frac{D_n}{\tau_n}}.\frac{A_p}{N_A}+\sqrt{\frac{D_p}{\tau_p}}.\frac{A_n}{N_D}\right) \tag{42}$$

Where the diffusion current due to carriers generated in the p and n regions is given by the first and second terms, respectively. In relation $n_i$ is the intrinsic carrier concentration ,$\tau_n$ ($\tau_p$) is the minority carrier diffusion in lifetime the p (n) material , and $A_P$ ($A_n$) is the area of the depletion region boundary in the p(n). Material Also, $N_A$ and $N_D$ are the doping densities, and $D_n$, $D_P$ are the minority carrier diffusion constants in the p and n regions respectively. The diffusion constants are obtained from the appropriate carrier mobilities μ using the Einstein relation D/μ = KT/q.

*b) Generation-Recombination current*

The current due to generation and recombination of electron-hole pairs in the depletion region is approximately [14]:

$$I_{gr} = \frac{qn_iAW}{\tau_{eff}}[\exp(\frac{qV}{2kT})-1] \tag{43}$$

where $\tau_{eff}$ is the effective carrier lifetime and $V$ is negative under reverse bias.

*c) Tunneling Current*

Tunneling dominates the dark current at high voltage, and is given for direct gap semiconductors by this relation [14]:

$$I_{tun} = \gamma A\exp\left(-\frac{2\pi\Theta m_0^{1/2}E_g^{3/2}}{qhE_m}\right) \tag{44}$$

$$\Theta = \alpha\left(m_C^*/m_0\right)^{1/2} \tag{45}$$

$$\gamma = \left[\frac{2m^*}{E_g}\right]^{1/2}\left(\frac{q^3E_mV}{4h^2}\right) \tag{46}$$

Where $m_0$ is the free electron mass, h is Planck constant and $E_m$ is the maximum junction electric field given by $E_m = -2(V+V_{bi})/W$. The parameter Θ is a dimensionless quantity given by here (45). $m_c^*$ is the effective mass of the electron, and α depends on the detailed shape of the tunneling barrier and is on the order of unity for band-to-band processes. The prefactor γ depends on the initial and final states of the tunneling carrier. For tunneling via traps in the bandgap, γ would depend on the density of traps and therefore

differs somewhat from its value for band-to-band tunneling.

*2) Dark Current Calculation in MQW-Region*

$I_{dark}$ in the absorption region is the sum of thermionic emission $I_{TE}$, and tunneling $I_{tun}$ components. The termionic emission dark current plays a more important role than the tunneling dark current. The confined electrons can escape from the well through thermionic emission. The current across a single well-barrier cell due to the thermionic emission at a temperature $T$ can be written [9]:

$$I_{TE} = SA^{*}T^{2}\, exp(\frac{-\phi_b}{kT})[exp(\frac{qV_{app}}{kT})-1] \qquad (47)$$

Where $S$ is the active surface of the diode, $A^*$is the Richardson constant, $T$ is the temperature, $\varphi_b$ emission barrier related to the barrier height, $k$ is Boltzmann's constant, $q$ electrical charge on one electron, and $V_{app}$ the applied voltage.

## IV. Results

To examine the accuracy of the model, we compare the results obtained from the model with the experimental results. As an example, an InP/InGaAs SACM-APD have been simulated [14]. Parameters needed in the model are mainly same as [8]-[16]. The simulation results for the photocurrent have been compared with the experimental results in Fig.8. It can be seen that the simulation agrees with the experiment. The differences between simulation and experiment results from our assumptions. Fig.9 shows the simulation and experimental results for the dark current. For low bias, the dark current is dominated by the diffusion and generation-recombination current, and for higher bias, the tunneling current plays an important role. Also the dark current is increased with bias voltage because of the higher electric field. From the above results, we conclude that the presented model is capable of predicting the behavior of SACM-APD.

We compare the results obtained from the MQW-SACM-APD model with the SACM-APD results. As an example, an InP/ $In_{0.53}Ga_{0.47}As$ SACM-APD which employ MQW structure in absorption region have been simulated. Parameters needed in the model are mainly same as [8]-[16]. The simulation results for the photocurrent have been compared with the SACM-APD simulation results in Fig.10. It can be seen from simulation results the photocurrent has been increased. Fig.11 shows the simulation results at four different wide wells.

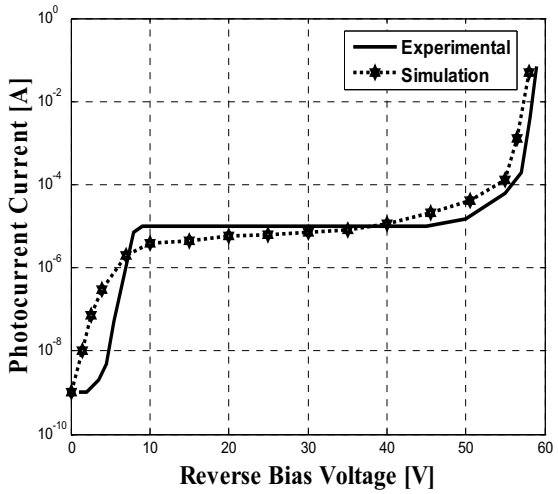


Fig.8.Comparing the simulation result for the photocurrent versus Reverse Bias with experiment [15].

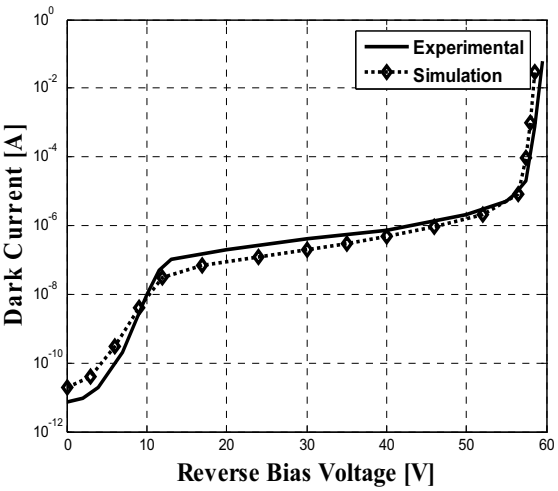


Fig.9. Comparing the simulation result for the dark current versus Reverse Bias with experiment [15].

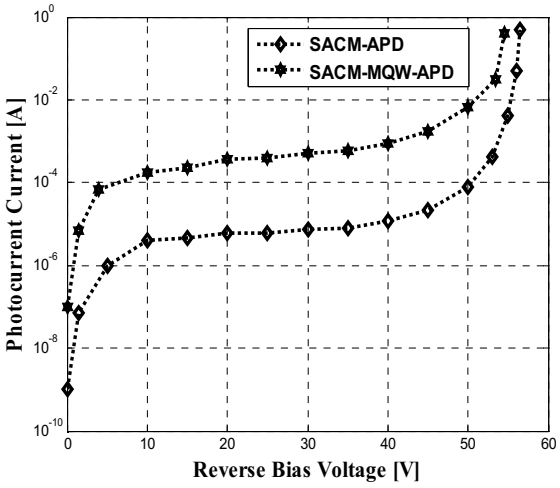


Fig.10. Comparing the simulation result for the SACM-APD with MQW-SACM-APD.

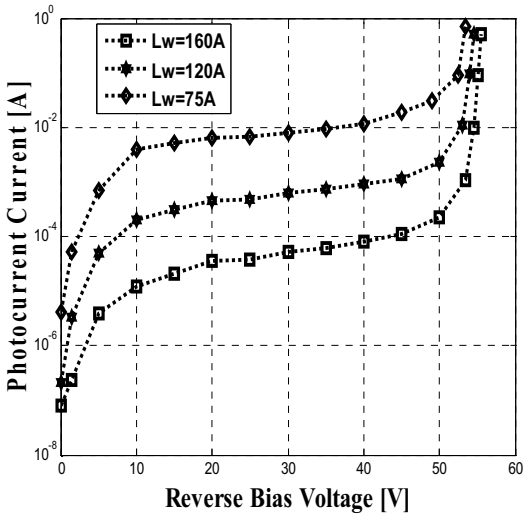


Fig.11. Simulation result for the photocurrent versus Reverse Bias for MQW-SACM-APD at 4 different wide wells.

## V. Conclusion

A new physical model for MQW-SACM-APD has been presented under some reasonable assumption. In this model we have considered the nonuniformity of electric field in active region. This process has been implementation with splitting the active region of device into smaller pieces and for each region we assumed that the profile of electric field is changed step by step. Using this model, we calculated the photocurrent and dark current. By this model device parameters can be optimized very fast.

## VI. Acknowledgment

Authors acknowledge for fractional financial by Iran Telecommunication Research Center.

## References

[1] J. C. Campbell, "Recent advances in telecommunications avalanche photodiodes," *Lightwave. Tech. J*., vol. 25, no. 1, Jan. 2007.

[2] S. D. Personick, "Receiver design for digital fiber-optic communication systems," *Bell Syst. Tech. J*., vol. 52, pp. 843-866, 1973.

[3] B. L. Kasper and J. C. Campbell, "Multigigbit-per-second avalanche photodiode lightwave receivers," *Lightwave. Tech. J*., vol. LT-5, pp. 1351-1364, 1987.

[4] Y. Kang, P. Mages and A. R. Glawson, ''Fused InGaAs-Si avalanche photodiodes with low-noise performances," *IEEE Photonic Tech Lett*, vol. 14, no. 4, pp. 1593-1595, 2002.

[5] F. Ma, S. Wang, and X. Li; "Monte Carlo simulation of low noise avalanche photodiodes with heterojunction," *Appl. Phys. Lett*., vol. 92, no. 2, pp. 4791-4795, 2002.

[6] Y. Zhao, S. He, "Multiplication characteristics of InP/InGaAs avalanche photodiodes with a thicker charge layer," Optical Communications 265, pp. 476-480, 2006.

[7] A. Zarifkar and M. Soroosh, "Circuit modeling of separate absorption, charge and multiplication avalanche photodiode (SACM-APD)," *6th International Conference on Laser and Fiber-Optical Network Modeling (LFNM)*, pp. 213-219, Ukrain, 2004.

[8] W. Chen, Sh. Liu, "PIN avalanche photodiodes model for circuit simulation," *IEEE J Quantum Electron*., vol. 32, no. 5, pp. 2105-2111, 1996.

[9] M. Wintrebert-Fouquet and B. Orsal, "Temperature investigation of dark current and its electrical noise in GaAs/AlGaAs multiquantum well photodiodes," *J. Appl. Phys*., vol. 85, no. 2, Jan. 1999.

[10] T. H. Wood, "Multiple quantum well (MQW) waveguide modulators," *Lightwave. Tech. J*., vol. 6, no. 6, June. 1988.

[11] A. K. Ghatak, K. Thyagarajan and M. R. Shenoy, "A novel numerical technique for solving the one dimensional schroedinger equation using matrix approach-application to quantum well structures," *IEEE J. Quantum Electronics*., vol. 24, no. 8, Aug. 1988.

[12] G. Lengyel, K. W. Jelley and R. W. Engelmann, "A semi-empirical model for electroabsorption in GaAs/AlGaAs multiple quantum well modulator structures," *IEEE J. Quantum Electronics*., vol. 26, no. 2, Feb. 1990.

[13] P. Bhattacharya, *Semiconductor Optoelectronic Devices*, Prentice-Hall, 1997, pp. 135-138.

[14] S. R. Forrest, "Performance of $In_xGa_{1-x}As_yP_{1-y}$ photodiodes with dark current limited by diffusion, generation recombination, and tunneling," *IEEE J. Quantum Electron*, vol. QE-17, pp. 217-226, 1981.

[15] D. Hasko, "InGaAs/InP avalanche photodiode with seperated absorption, charge and multiplication layers," *International Student and Young Scientists Workshop "Photonics and Microsystems"*, 2004.

[16] S. Adachi, *Physical Properties of III-V Semiconductor Compounds*, New York: Jhon. Wiley, 1992, PP. 246-247.